# Geometrical Characterization of an Inorganic Scintillator Detector for Proton Therapy using a Micrometer Scale Ion Beam

Kévin Lalanne, S.B.C. Debnath, G. Simonin, D. Tonneau, François Vianna-Legros, Marc Rousseau, David Brasse, J. Darréon, Carole Fauquet

# Geometrical Characterization of an Inorganic Scintillator Detector for Proton Therapy using a Micrometer Scale Ion Beam

K. Lalanne, S.B.C. Debnath*, G. Simonin, D. Tonneau, F. Vianna-Legros, M. Rousseau, D. Brasse , J. Darréon, and C. Fauquet

***Abstract*— The fabrication process of an Inorganic Scintillator Detector (ISD), grafted at the tip of an optical fiber, is currently under optimization for its application in proton therapy in-vivo dosimetry. The detector signal magnitude under proton irradiation is strongly correlated to the geometry of the detector-sensitive head and must be accurately characterized. This parameter is also essential for detector response calculation using Monte Carlo(MC) simulation. The purpose of this work is to get a luminescence map of the ISD scanned with a 4 MeV $H^+$ microbeam. The beam is tightly focused on a spot with a diameter of 2.2 µm at a distance of 250 µm working distance, or 4.9 µm and 32.5 µm at distances of 1 and 4 mm, respectively. The beam scans the detector in a raster scan mode. The luminescence signal emitted locally by the detector is collected via the optical fiber and measured using a photon counter. The results provide insights into the geometry of the efficient volume of the detector without damage, making this technique particularly suitable for non-destructive characterization.**

***Index Terms*— Proton beam, Dosimetry, Biomedical applications of radiation, Luminescence, Luminescent devices, Radiation detectors, inorganic detector, Optical fiber devices, Particle beam measurements, Radiation dosimetry, X-ray detectors, X-rays.**

## I. Introduction

In recent years, a strong attention has been focused on proton therapy (PT) for cancer tumor treatment [1, 2]. More than one hundred proton beam medical centers have emerged around the world in the last decade [3, 4]. This therapy offers several advantages over conventional radiotherapy techniques including very high dose conformity with the targeted volume, and the possibility for a lower dose deposition in the healthy tissues around the beam path. Thus, organs at risk are preserved from unnecessary irradiation [5].

Similar to other radiation techniques, the undesirable effects of proton therapy include non-reparable cell damage [6], necrosis of the surrounding tissues, and undesirable biological effects on healthy tissues [7]. In this context, quality assurance in the dose distribution is vital to reduce the difference between the dose calculated by the treatment planning system (TPS) and the dose delivered to the targeted tumor volume by the therapy equipment.

Proton beam dosimetry has been performed by different well-known organic plastic scintillator-based detectors [8-11,25], as well as silicon-based radiation detectors [12]. Plastic detectors are water equivalent and are thus widely used in dose measurement and monitoring. However, despite recent improvement of their luminescence yield, it is still difficult to use them as 3D sub-millimeter devices for lateral high resolution beam profiling. Moreover, non-linearities due to quenching effects [8, 13, 14], Cerenkov emission contribution, and volume averaging effects [8] hinder their use for proton beam dosimetry. Inorganic Scintillator Detectors (ISD) are promising in various applications using low- or high-energy X-rays, proton, and hadron therapeutic beams [16,17,18,25-26]. They were successfully evaluated for these applications as well as for intensity-modulated proton therapy (IMPT) [16, 22].

The purpose of the present work is to characterize the geometry of a compact inorganic scintillator detector. The luminescence front and lateral maps of the detector using a

This article was submitted on the 13th day of Nov 2023.
(S.B.C Debnath and K. Lalane are co-first authors. Asterisk indicates corresponding author.)

Dr. Sree Bash Chandra Debnath is a MSCA global post-doctoral research fellow at Aix-Marseille University-CNRS. sree.debnath@univ-amu.fr

Dr. Kevin Lalanne is a research engineer at Institut de radioprotection et de sûreté nucléaire (IRSN), Cadarache. kevin.lalanne-crit-interim@irsn.fr

Mr. Gael Simon is PhD student at Institut Pluridisciplinaire Hubert Curien – Strasbourg. gael.simonin@iphc.cnrs.fr

Prof. Didier Tonneau is a Full Professor in Physics, Aix-Marseille University and Head of X-tip research group, CINaM. didier.tonneau@univ-amu.fr.

Dr. F. Vianna-Legros is a Researcher at IRSN, Cadarache. francois.vianna-legros@irsn.fr

Dr. Marc Rousseau is an associate professor at Institut Pluridisciplinaire Hubert Curien (IPHC), CNRS, Strasbourg. marc.rousseau@iphc.cnrs.fr

Dr. David Brasse is a Research Director at Institut Pluridisciplinaire Hubert Curien (IPHC), CNRS, Strasbourg. david.brasse@iphc.cnrs.fr

Dr. Julien Darreon is a Medical Physicist at Paoli-Calmettes Institute in Marseille, France. darreonj@ipc.unicancer.fr.

Dr. Carole Fauquet is an associate professor in Physics, Aix-Marseille University- CINaM, CNRS, France. carole.fauquet@univ-amu.fr.

This article has been accepted for publication in IEEE Sensors Journal. This is the author's version which has not been fully edited and
content may change prior to final publication. Citation information: DOI 10.1109/JSEN.2024.3401630



highly focused proton microbeam at an energy of 4 MeV are presented and discussed. The geometry of the detector sensitive part has been characterized. The detector response with respect to the incident beam flux is also presented.

## II. Experimental Details

### A. MIRCOM Facility

The experimental work was performed at the IRSN's MIRCOM facility, equipped with a horizontal ion microbeam. It is located at Cadarache Research Center (Saint-Paul-lès-Durance, France), and is operated by the micro-irradiation, neutron metrology, and dosimetry laboratory (LMDN) from the Health and Environment Division of the Institute for Radiological Protection and Nuclear Safety (IRSN, France). It delivers several micrometer-scale ion beams, namely $H^+$ and $He^{2+}$, or heavier ions, such as $C^{3+}$, and $O^{3+}$. Before entering the beamline, the ions are accelerated by a 2 MV TANDETRON™ accelerator, manufactured by High Voltage Engineering Europa (HVEE, The Netherlands), operating up to 4 MeV for protons (ions used in this study), and up to 6 MeV for alpha particles ($He^{2+}$), up to 8 to 12 MeV for heavier ions ($C^{3+}$ and $O^{3+}$), depending on their charge state. The ion flux is measured using an external PIPS (Passivated Implanted Planar Silicon) detector facing the beam. The uncertainty on the measurement is equal to the square root of the event number.

MIRCOM facility is user-friendly and suitable for radiobiology experiments, and it is currently used to irradiate multicellular organisms, cells, and even sub-cellular elements [19-21]. In order to avoid the damage of the thin extraction window, a minimum working distance (distance from extraction window to sample) is set at 250 µm. The profile of the proton beam was determined through irradiations on a CR39-type trace detector and on cells (U2OS). The average impact diameter is 2.2 ± 0.3 µm at 250 µm, in good agreement with 2.1 ± 0.7 µm (targeting accuracy value) [19]. The beam diameter, calculated using the SRIM software is 4.9 µm and 32.5 µm at working distances of 1 mm and 4 mm, respectively. These values will be used in this study.

### B. Inorganic Scintillator Detector (ISD)

We have fabricated a detector based on an inorganic scintillator, particularly suitable for real-time dosimetry. The detector is composed of a 10-meter-long silica multimode optical fiber ended by a polymer 'bulb' embedding(Zn,Cd)S: Ag micrometer-size clusters [17,18]. The optical fiber (THORLABS- FG105LVA) has core and cladding diameters of 105 and 125 µm, respectively. The transmission bandwidth is 400-2100 nm, and the numerical aperture (NA) is 0.1 (acceptance half angle, 5.7°, fiber design data). Bulb irradiation by protons leads to visible luminescence that is guided by the optical fiber to a sensitive photon counter (Aurea Technologies™) with intrinsic dark noise of about 50 photons/s. The dark count (when the beam is off, or on but does not irradiate the bulb) is 350 photons/s. All the presented results here are corrected for the dark count. The fluctuations of the whole measurement chain during experiments (comprising the device, fiber, and the photon counter), are ± 150 photons/s. The integration time of photon counter was 1s. The signal was only observed when we irradiated the scintillating part of the ISD and remained at the background level when the fiber was directly irradiated (outside the bulb). No significant fiber photodarkening could be observed during the total irradiation time including the time necessary for alignment.

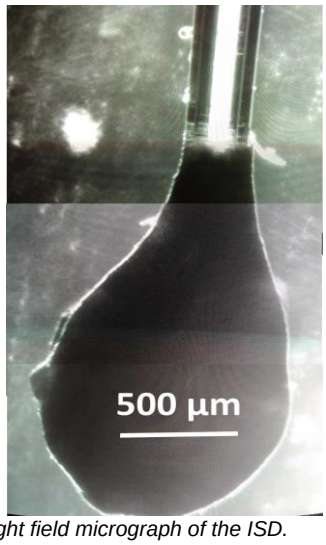


Fig. 1. *Optical bright field micrograph of the ISD.*

Figure 1 presents an optical bright field image of the ISD. The bulb , at the fiber tip has an ellipsoidal shape of dimensions a, b, and c along respective axes X, Y, and Z (see figure 2).

The luminescence mapping of the detector can be conducted using either axial irradiation (as shown in Figure 2, configuration (a)) or lateral irradiation (Figure 2, configuration (b)). In both scenarios, the X-axis corresponds to the beam axis, while the fiber axis is X or Z, depending on the specific

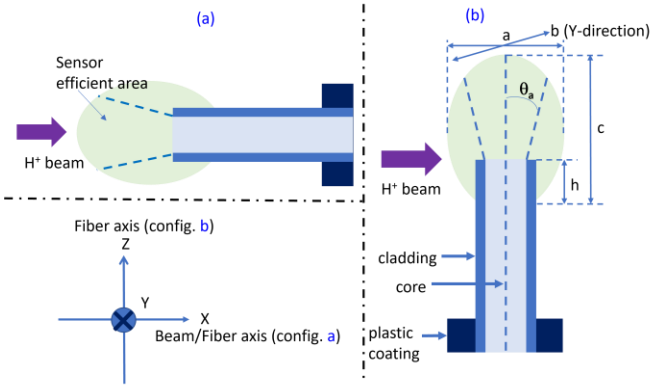


Fig. 2. Schematic of the detector cross-section within a plane containing the fiber axis. (a) front/axial irradiation, and (b) lateral irradiation. a, b and c are the dimensions of the detector along X, Y, and Z axis. h is the penetration depth of the fiber inside the sensor. The acceptance angle, $\theta_a$ of the fiber is approximately 5.7° (Numerical aperture of 0.1). The X axis is chosen as the beam axis in both configurations. The fiber axis is: (a) X, (b) Z. [The figure does not necessarily depict the true dimensions]

configuration (a) or (b). Figure 2(b) presents a sensor schematic highlighting the different parts of the detector: the ellipsoidal luminescent bulb, the optical fiber cladding, and core. The fiber has a very low numerical aperture and only a slight part of the total 4π luminescence of the bulb can be collected and transmitted by the fiber. This luminescence comes only from a truncated cone determined by the fiber core acceptance angle. Any light emitted outside of this efficient volume theoretically cannot be collected by the fiber and therefore cannot be transmitted to the photon counter.This region is referred to as the 'efficient volume' in the following.

### C. ISD Characterization

Under irradiation with a conventional wide therapeutic beam, the collected luminescence signal is expected to increase with the volume of the sensor's efficient zone. This specific parameter relies on the penetration length (length h-figure 2(b)) of the fiber into the bulb and cannot be characterized by a non-destructive microscopy technique. To determine this parameter, we have recorded luminescence maps of the bulb during the proton beam raster scan. Two configurations were studied to achieve front and lateral maps (Figures 2a and 2b). These measurements were carried out by keeping the proton beam stationary while moving the sensor in a plane perpendicular to the microbeam. The step size was configured at 10 µm for front irradiations and 20 µm for lateral irradiations. The proton beam flux remained constant at 2780 ± 53 protons/s during experiments. The experiments were repeated at least 2 times. The beam-detector alignment is difficult because no visual access was possible. Thus, several scans were needed to position the luminescence map in the center of the figures. The maximum value read on the photon counter did not change during the whole process of alignment and imaging. No further statistics were performed.

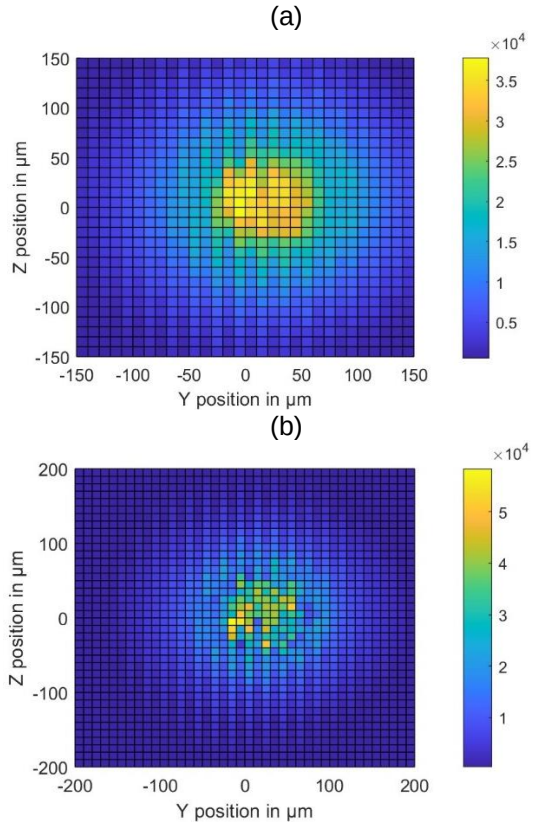


Fig. 3. Luminescence map of the ISD sensor using front irradiation. The scan step is 10 µm in both Y and Z directions. The X-axis is the beam axis. The ISD to extraction window distance is (a) 4 mm and (b) 1 mm.

## III. Results and Discussions

### A. Front Irradiation

First, experiments were carried out in front irradiation, positioning the detector at a working distance of 4 mm. At this distance, the beam diameter is 32.5 µm. In this case, the signal map exhibits a 3D Gaussian-like profile with a maximum of 37.5 x$10^3$ photons/s. The top view of the map is given in Figure 3a. The luminescence map has a FWHM of 100 ±10µm, in good agreement with the fiber core diameter (105 µm ± 3 µm, design data).

Subsequently, the ISD was approached toward the extraction window, reducing the working distance to 1 mm. In these conditions, the beam diffusion in the air decreases. Thus, the beam probe size is shrunken down to 4.9 µm. The map follows a 3D-Gausssian like profile with a FWHM of 98 ±10µm. A top view is shown in Figure 3b. The maximum flux of 58.3x$10^3$ photons/s is achieved when the beam is aligned with the fiber axis. The profile exhibits more irregularities compared to what is shown in figure 3a. This is likely attributed to the non-uniformity of the dosimeter, which becomes more apparent when using a smaller probe. In contrast, when using a wider probe, the detector integrates the signal over a larger surface, which helps to smooth the non-uniformities in the sensor. These experiments confirm that the most efficient volume of the bulb is the zone limited by the acceptance cone of the fiber.

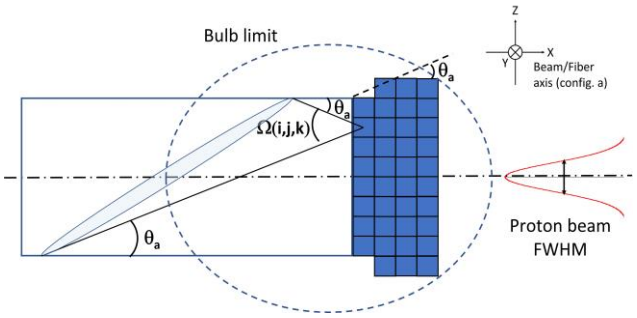


Fig. 4. Simulated system used for photometric considerations. A Gaussian-shaped proton beam (on the right) irradiates an ellipsoidal ISD. The model is based on semi-finite element methods and the ISD is divided in cubic unit cell emitting visible luminescence in 4π directions. The fiber collects a part of the emission of each (i, j, k) cell, limited by the fiber acceptance $\theta_a$, within a solid angle Ω(i,j,k).

The maximum signal achieved when the beam is aligned with the fiber axis is 55% higher when the proton beam diameter is shrunken from 32.5 µm to 4.9 µm. In both cases, the protons are totally stopped in the detector and thus, the total energy deposited is the same, leading to the same 4π total visible emission. Photometric calculations have been carried out to estimate the photon number collected by the fiber aperture as a function of proton beam diameter. The system was simulated as presented in Figure 4. A Gaussian-shape proton beam irradiates the detector along the optical fiber axis. This position leads to the maximum luminescence signal. The model is based on a semi-finite element method and ISD is divided in cubic unit cells of side s = 0.1 µm. Under irradiation, each cell emits visible light in 4π steradians from its center, positioned at (i.s, j.s, k.s) along X, Y, Z axis, respectively. The fiber collects only a small part of this emission, given by the solid angle Ω(i, j, k) limited by the fiber acceptance angle $\theta_a$. The system exhibits a symmetry of revolution around the fiber axis. From this, the emitted light yield transferred to the photon counter can be calculated as a function of proton beam diameter. Simulations show that the maximum signal increases of 41%, if the beam decreases from 32.5 to 4.9 µm. The signal increase should thus be mainly attributed to photometric considerations.

However, calculations show that a flux of 40 electrons, with an energy lower than 8.7 keV, are produced for 1000 incident protons interacting with the extraction window. Their maximum mean free path in the air is about 2.3 mm. So, those electrons can hit the detector at the smallest working distance and could participate in the luminescence increase observed at a 1mm working distance. Other particles (neutrons and X rays) are produced by the window in negligible amounts.

### B. Lateral Irradiation

The experiments were also performed under lateral irradiation (Figure 2b). Figure 5 shows the sensor map obtained by a 2D scan of the detector by the microbeam. The step was 20 µm in both Y and Z directions. Figure 5a shows a two-color map with a threshold set at 1.2 x $10^3$ visible photons/s, corresponding to about 4 times the background level when the proton beam is switched off. We estimated that this level is significant enough to ensure that the beam hits the bulb. We observe that the bulb is a quasi-ellipsoid with b (= a) and c dimensions of 325 µm and 600 µm, smaller than the dimensions obtained by optical microscope analysis (see Figure 2). Even if the beam hits the surface outside the efficient volume, a significant signal is detected by the photon counter. To address this issue, figures 5b to 5f present the same sensor maps with thresholds respectively chosen at $2x10^3$, $5x10^3$, $8x10^3$, $10x10^3$, and $20x10^3$ photons/s. In figure 5b we can observe that the detector outline giving a significant signal (6 times the background) is smaller than this obtained at a lower threshold. Figure 5c, at a higher threshold, confirms this trend. Moreover, no signal higher than $5x10^3$ photons/s is observed in the left part of the figure when the beam impinges the detector around Y=0 axis. This trend is emphasized when the threshold is further increased (figures 5d and 5e). The shape and size of this zone are in good agreement with the fiber core itself. Finally, with a threshold set at $10x10^3$ or $20x10^3$ photons/s, we clearly see in figures 5e and 5f that a high-level signal is only collected when the beam hits the bulb at the fiber core tip corresponding to the detector's most efficient area. The maximum signal collected at this position is $92x10^3$ photons/s. The thickness of this region extending from the core fiber ranges between 80 µm and 100 µm (Figure 5f), value significantly smaller than the total bulb height c (figure 2b). By comparison between figures 5a and 5f, fiber tip can be estimated at a distance of 100 to 120 µm from the physical extremity of the detector (c-h value in Figure 2b).

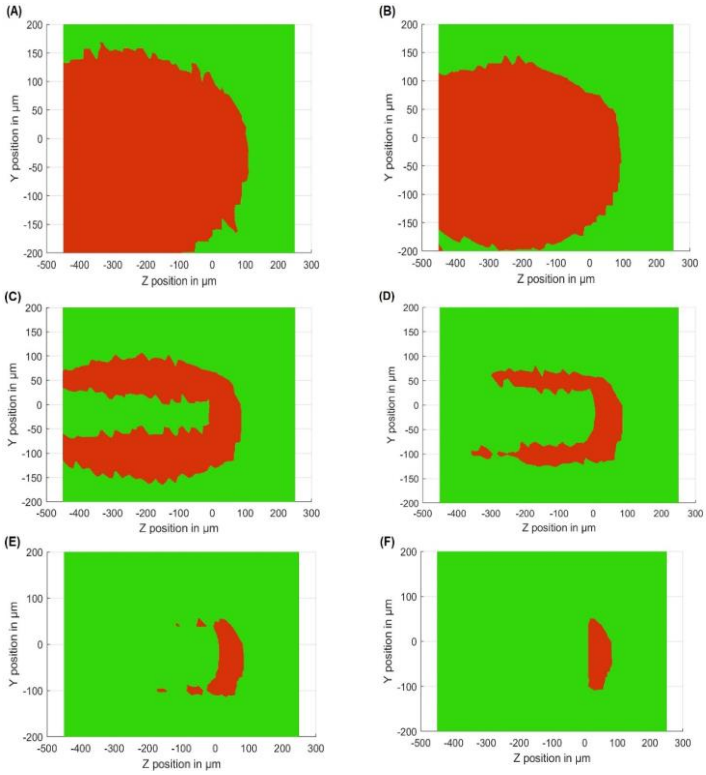


Fig. 5. Signal detected on the photon counter as a function of the position of the microbeam on the detector during a 2D scan at various thresholds: (a) $1.2x10^3$ photons/s, (b) $2x10^3$ photons/s, (c) $5x10^3$ photons/s, (d) $8x10^3$ photons/s, (e) $10x10^3$ photons/s, and (f) $20x10^3$ photons/s

### C. Luminescence signal vs proton beam position

Figure 6 shows the raw data obtained by line scans of the beam at five different Z positions $Z_a$ to $Z_e$ along fiber axis (Z-axis). The detector is not symmetrical, so experimental curves cannot present any symmetry, and the lines on this figure just serve as visual guides. If the beam hits the sensor almost tangentially to the bulb (profile (a)), the resulting profile exhibits a gaussian-like shape. A maximum signal of $32x10^3$ photons/s is achieved when the beam points towards the effective efficient volume. The full width at half maximum is 100 µm, that corresponds to the diameter of the fiber core. The lateral profile recorded closer to the fiber tip (profile (b)) also presents a Gaussian shape but with a higher maximum value (about $92x10^3$ photons/s). If the beam crosses both fiber core

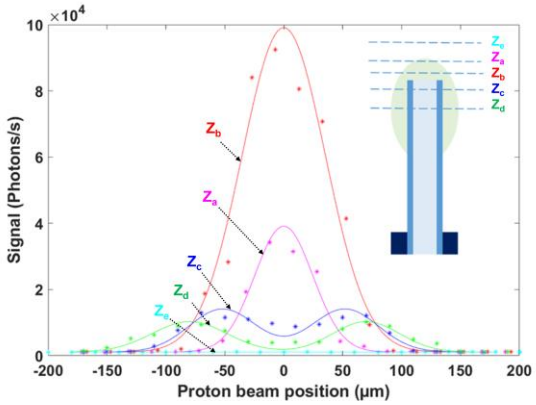


Fig. 6. Luminescence signal variations with proton beam impact position on the bulb along Y axis in different Z-planes (a) the proton beam scans nearby the bulb end, (b) beam crosses the head nearby the fiber core tip, (c) beam crosses the fiber core and cladding, (d) beam crosses fiber core and cladding far from fiber tip, (e) beam scans just above the bulb. The lines serve as visual guides.

and cladding, the lateral profile exhibits a "volcano" shape (profile (c)). If the beam hits the detector at a farther distance from the fiber tip, the profile remains similar with the same "crater" height but with a deeper "volcano chimney" (profile (d)). If the beam crosses the fiber axis, the signal is nearly equal to the background level and achieves 350 photons/s. If the beam hits the sensor around the fiber cladding, a signal of $10x10^3$ photons/s is recorded for c and d profiles. Finally, the profile recorded far from the dosimeter end is flat, and the signal remains at the background level (profile (e)).

Visible photons can be collected by the photon counter only if they come from the efficient zone within the fiber acceptance angle. If the beam crosses the bulb in the efficient volume, the energy deposited by the protons travelling through the detector is maximum and a maximum signal is obtained. However, if the beam does not hit the detector in the efficient volume, the photon counter unexpectedly collects some visible light. Several phenomena could explain this observation. First, a part of this unexpected light could be due to the scattering/reflection of visible photons within the non-homogeneous detector. Secondly, interaction of protons with the detector might generate atom ionization and/or excitation, leading to the emission of electrons and fluorescence photons [23,24].Some of these particles can possibly cross the efficient volume of the detector and generate visible photons. To evaluate the number of X-rays and electrons generated in the bulb by protons, a Monte Carlo simulation was performed using the GATE platform version 9.1 [27]. The simulation parameters used are summarized in table 1.

Table1: Parameters used in GATE simulation.

| Parameter | Value |
|---|---|
| Physics list | QGSP_BIC_HP_EMY |
| DEDX table binning | 25 bins/decade |
| Production threshold $\gamma, e^-, e^+$) | 0.1 $\mu m$ |
| Maximum step ($p^+$) | 1 $\mu m$ |
| No. of primary protons | 50 x $10^6$ |

The simulated source was a 4 MeV monoenergetic proton beam with no divergence. This source irradiates a cubic phantom of scintillator/PMMA mixture corresponding to the ISD composition.

Calculations provide the projected range of protons within the phantom and the energy spectrum of generated electrons and X-rays. These spectra were used as a source in a second simulator to evaluate the range and the attenuation length of these particles inside the detector.

As shown in Table II, secondary electrons or photons generated by protons have low energy, and are stopped before reaching the detector's efficient volume.

Protons can also generate neutrons or g-rays by nuclear interaction [28]. By considering the possible interactions between 4 MeV protons and the elements in the bulb producing neutrons [29], it was possible to estimate that for 100 incident protons, around 1.1 to 1.6 neutrons are produced in the interaction volume. This corresponds to the formation of 33 to 50 neutrons/s for a 2780 $s^{-1}$ proton flux. The ratio of 0-4 MeV neutrons that can travel far and so can lose substantial energy far from where they were produced is less than 2%. Consequently, it corresponds to a flux of 0.66 to 1 neutron.$s^{-1}$. According to the large mean free path of neutrons, these particles can achieve the efficient volume of the detector and induce a part of this unexpected luminescence. γ-rays are probably at the origin of the balance of the signal.

Figure 7 shows a schematic of the sensor cross section perpendicularly to the fiber axis (Z-axis). In figure 7(a), the section does not cross the fiber. If the beam is at coordinate $Y_a$, most probably, the Bragg peak is located within the detector efficient volume and the signal is maximum. When the beam is progressively moved to $Y_c$ position, the thickness encountered by the beam decreases and the proton energy loss in the detector decreases. Thus, the signal decreases. Finally, when the beam is at $Y_d$ position, the thickness becomes too low, and the protons do not lose enough energy to generate detector luminescence. This explains the Gaussian-like luminescence profiles a and b shown in figures 6. The higher maximum signal recorded at $Z_b$ position (inset, figure 6) is due to a longer path of the beam into the bulb than if the beam is at position $Z_a$. If the proton path length in the bulb is too short (beyond $Y_d$ position in figure 7a), the visible signal produced will not be significant because the energy loss is too small. This explains why the luminescence map shows smaller extent than the actual detector's geometrical dimensions.

In figure 7(b), the section crosses the optical fiber. In this case, the luminescence signal detected is indirectly generated by the detector efficient volume, because the beam does not cross this volume. In that case, the proton path length through the scintillating part of the detector increases from beam

position $Y_a$ to $Y_c$, achieves a maximum at this position, and then decreases till the beam reaches the detector's physical end. It is thus expected that the energy deposited by the proton

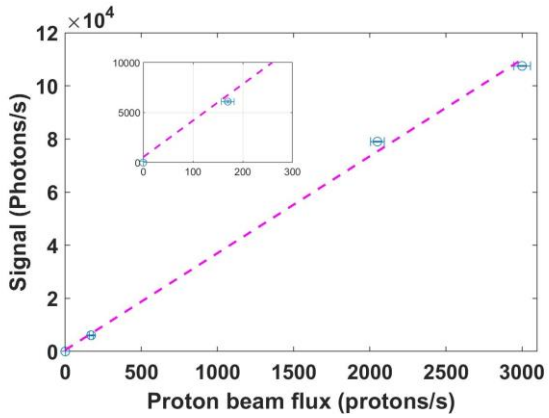


Fig. 8. Variation of photon counter signal with incident proton beam flux.

beam first increases and then decreases from $Y_a$ to $Y_d$ positions. In this case, the visible photons emitted by proton slowdown are probably produced by neutrons and/or γ-rays that reach the efficient volume. A part of the total visible emission can thus be collected by the fiber and transferred to the photon counter. This phenomenon occurs on both sides of the fiber and explains the origin of the "volcano-like" profile observed in figure 6 ($Z_c$ position). The maximum signal is expected when the beam is positioned tangentially to the optical fiber, where the proton path is larger, at $Y_c$ position (Figure 7b). Moreover, in position $Y_a$, the bulb is too thin to stop the beam and the protons penetrate the fiber cladding and core where they are stopped. Indeed, it would be possible to detect a significant luminescence signal if the beam crossed the fiber cladding and core and were stopped behind the core. That is not the case (see Figure 5c to 5f). This allows the exclusion of direct fiber strong excitation by the proton beam and high Cherenkov luminescence emission in the fiber core. If the proton beam is positioned close to the fiber tip(position $Z_c$, figure 6), scattered visible light can possibly reach the efficient volume of the detector, and a luminescence signal is collected. However, when the beam is positioned far from the fiber tip(position $Z_d$, figure 6), these scattered photons cannot reach the efficient volume and in that case the signal detected is probably due to neutrons/γ-ray generation. The "volcano-like" profile then becomes deeper.

### D. Signal Variations vs Proton beam Flux

Figure 8 shows the variations of the optical signal with respect to the proton beam flux. During these experiments, the detector was laterally irradiated (configuration 2(b)). The signal is proportional to the incident proton flux, with a yield of 36 collected photons per incident 4 MeV proton. Because the photon counter is highly sensitive (less than 10 photons/s), it is realistic to assert that achieving proton-by-proton flux control at this energy is feasible using this detector.

The distance between the fiber tip and the detector's physical end is about 100 µm to 120 µm. Additionally, it is observed that if the beam tangentially hits the dosimeter's fiber core surface, the path length before protons reaches the efficient volume is about 50 µm. The mean energy loss per

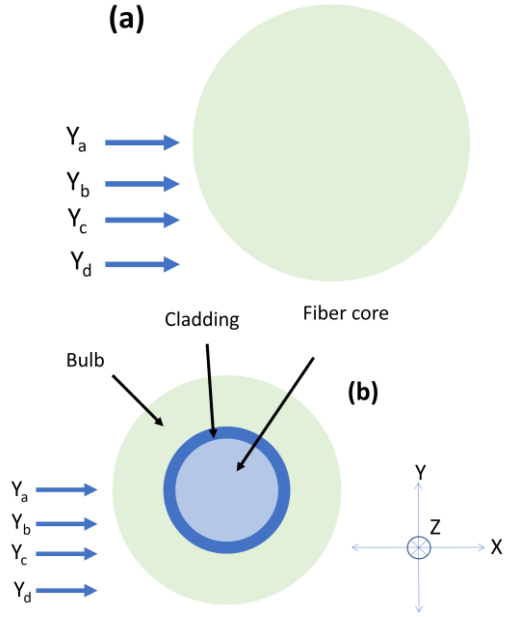


Fig. 7. Schematic of the sensor cross section in a plane perpendicular to the fiber axis. (a) section between detector apex and fiber core (b) section crosses both scintillating bulb and optical fiber.

distance traveled (dE/dx) and the total path length of a 4 MeV proton in the dosimeter are calculated to be 16.5 keV.µm$^{-1}$ and 160 µm, respectively. These values were calculated using the SRIM software, for a detector composition of 50% PMMA and 50% (Zn,Cd)S:Ag. Therefore, the energy of the proton is about 3.1 MeV when they reach the efficient volume. Moreover, all the protons are stopped inside this volume.

The luminescence is emitted in 4π directions, but the fiber captures only a small fraction of it. For a visible point source located just at the fiber tip, the collection is limited by the fiber acceptance angle θa (5.7° in our case). Consequently,

TABLE II
PARTICLE WITHIN GATE ENVIRONMENT

| | Maximum Energy (keV) | Most Probable Energy (keV) | Attenuation length of 90% particles (µm) |
|---|---|---|---|
| Electron | 8.7 | 1.5 | 0.20 |
| X-ray Photons | 7.6 | 0.26 | 0.75 |

Main characteristics of the particles generated by a 4- MeV protons stopped in the detector calculated within GATE environment. [The simulated source was a 4MeV monoenergetic proton beam with no divergence. Voxel size of 1 µm for photons and 0.01 µm for electrons were considered, and 50 million primaries were generated for each simulation.

less than 0.25% of the total emitted light is transferred to the photon counter through the fiber. Furthermore, because the counter collects 60% photons in the red emission range the total detector emission is 24 x$10^3$ emitted photons per incident proton at 3.1 MeV. In other words, the total 4π emission of the detector is approximately 8000 photons per deposited MeV. However, this rough approximation consider neither the quenching effect nor the visible light scattering by the grains inside the detector. This latter aspect is challenging to address without employing destructive imaging techniques such as SEM analysis of the detector's cross-section.

## IV. Conclusion

In this study, a 4 MeV proton microbeam was successfully used to probe and characterize the efficient zone of an inorganic scintillator detector. The luminescence mapping of the detector was performed by scanning it with the microscale beam in a raster scan mode, simultaneously recording luminescence collection with a visible photon counter. Frontal and lateral maps allowed us to define the geometry of the efficient zone of the detector and accurately determine its location inside the detector. Finally, our findings demonstrate that a proton-by-proton flux control can be achieved at a 4 MeV energy with this detector.

## Acknowledgment

The first two authors contributed equally to this work. This work was carried out with the financial support of A*MIDEX (# 2XTIPXIN/INTE/ID20HRU118), funded by the Investissements d'Avenir project funded by the French Government, managed by the French National Research Agency (ANR). It was also supported by ANR through Nanoptix project (#ANR-18-CE42-0016-02).

## References

[1] Yuan, Tai-Ze, Ze-Jiang Zhan, and Chao-Nan Qian. "New frontiers in proton therapy: applications in cancers." Cancer Communications 39: 1-7, 2019.

[2] Mohan, R., & Grosshans, D. Proton therapy–present and future. Advanced drug delivery reviews, 109, 26-44, 2017.

[3] PTCOG 2017. Hadrontherapy facilities worldwide in operation. www.ptcog.ch, (updated in January 2017).

[4] Grau, C.; Durante, M.; Georg, D.; Langendijk, J.A;Weber, D.C. Particle therapy in Europe. Molecular Oncol. 2020, 10, 142–149.

[5] Schardt D, Elsässer T and Schulz-Ertner D, Heavy-ion tumor therapy: physical and radiobiological benefits Rev. Mod. Phys. 82 383–425, 2010.

[6] Paganetti H, (2010) The physics of proton biology Proton Therapy Physics 1st edn (Boca Raton, FL: CRC Press) pp 593–626

[7] Ten Haken, R.K.; Marks, L.B.; Bentzen, S.M.; Constine, L.S.; Deasy, J.O.; Eisbruch, A.; Jackson, A. Quantitative analyses of normal tissue effects in the clinic. Int. J. Radiat. Oncol. Biol. Phys. 2010, 10, 3, 1–160.

[8] Hoehr, C., Lindsay, C., Beaudry, J., Penner, C., Strgar, V., Lee, R., & Duzenli, C. (2018). Characterization of the exradin W1 plastic scintillation detector for small field applications in proton therapy. Physics in Medicine & Biology, 63(9), 095016.

[9] Beaulieu, L., & Beddar, S. (2016). Review of plastic and liquid scintillation dosimetry for photon, electron, and proton therapy. Physics in Medicine & Biology, 61(20), R305.

[10] Fratelli, I., Ciavatti, A., Zanazzi, E., Basiricò, L., Chiari, M., Fabbri, L., ... & Fraboni, B. (2021). Direct detection of 5-MeV protons by flexible organic thin-film devices. Science Advances, 7(16), eabf4462.

[11] Posar, Jessie A., et al. "Characterization of a plastic dosimeter based on organic semiconductor photodiodes and scintillator." Physics and Imaging in Radiation Oncology 14 (2020): 48-52.

[12] Rosenfeld, Anatoly B. "Novel detectors for silicon based microdosimetry, their concepts and applications." Nuclear Instruments and Methods in Physics Research Section A: Accelerators, Spectrometers, Detectors and Associated Equipment 809 (2016): 156-170.

[13] Torrisi, L. "Plastic scintillator investigations for relative dosimetry in proton-therapy." *Nuclear Instruments and Methods in Physics Research Section B: Beam Interactions with Materials and Atoms* 170.3-4 (2000): 523-530.

[14] Alsanea, Fahed, et al. "A real-time method to simultaneously measure linear energy transfer and dose for proton therapy using organic scintillators." Medical physics 45.4 (2018): 1782-1789.

[15] Boon S N 1998 *Dosimetry and Quality Control of Scanning Proton Beams* (Wageningen: Ponsen & Looijen BV)

[16] Safai, Sairos, Shixiong Lin, and Eros Pedroni. "Development of an inorganic scintillating mixture for proton beam verification dosimetry." Physics in Medicine & Biology 49.19 (2004): 4637.

[17] 'High resolution small-scale inorganic scintillator detector: HDR brachytherapy application S.B.C. Debnath, M. Ferre, D. Tonneau, C. Fauquet, A. Tallet, A. Goncalves, J. Darreon, Medical Physics (2020), http://doi.org/10.1002/mp.14727

[18] 'High spatial resolution inorganic scintillator detector for high-energy X-ray beam at small field irradiation', Sree Bash Chandra Debnath, Carole Fauquet, Agnes Tallet, Anthony Goncalves, Sébastien Lavandier, Franck Jandard, Didier Tonneau, Julien Darreon, Medical Physics (2019). https://doi.org/10.1002/mp.14002

[19] Vianna, F., Gonon, G., Lalanne, K., Adam-Guillermin, C., Bottollier-Depois, J.-F., Daudin, L., Dugué, D., Moretto, P., Petit, M., Serani, L., Such, J., & Gressier, V. (2022). Characterization of MIRCOM, IRSN's new ion microbeam dedicated to targeted irradiation of living biological samples. *Nuclear Instruments and Methods in Physics Research Section B: Beam Interactions with Materials and Atoms*, *515*(December 2021), 20–30. https://doi.org/10.1016/j.nimb.2022.01.007

[20] Bobyk, L., Vianna, F., Martinez, J. S., Gruel, G., Benderitter, M., & Baldeyron, C. (2022). Differential Recruitment of DNA Repair Proteins KU70/80 and RAD51 upon Microbeam Irradiation with α-Particles. *Biology*, *11*(11), 1652. https://doi.org/10.3390/biology11111652

[21] Sleiman, A., Lalanne, K., Vianna, F., Perrot, Y., Richaud, M., SenGupta, T., Cardot-Martin, M., Pedini, P., Picard, C., Nilsen, H., Galas, S., & Adam-Guillermin, C. (2023). Targeted Central Nervous System Irradiation with Proton Microbeam Induces Mitochondrial Changes in Caenorhabditis elegans. *Biology*, *12*(6), 839. https://doi.org/10.3390/biology12060839.

[22] Debnath, S. B. C., Tonneau, D., Fauquet, C., Tallet, A., Goncalves, A., & Darreon, J. (2021). Dosimetric characterization of a small-scale (Zn, Cd) S: Ag inorganic scintillating detector to be used in radiotherapy. *Physica Medica*, *84*, 15-23.

[23] Alan Nahum, Ch. 3 Interactions of charged particles with matter; pp 36-41 'Handbook of Radiotherapy Physics, Theory and

Practice, Ed by P Mayles, A. Nahum and J. C. Rosenwald, CRC Press, Boca Raton, Fl, 2007.

[24] Obodovskiy, I. (2015). *Fundamentals of radiation and chemical safety*. Elsevier.

[25] Kanouta, Eleni, et al. "Time-resolved dose rate measurements in pencil beam scanning proton FLASH therapy with a fiber-coupled scintillator detector system." *Medical Physics* 50.4 (2023): 2450-2462.

[26] García Díez, Miguel, et al. "Measurement of the bunch structure of a clinical proton beam using a SiPM coupled to a plastic scintillator with an optical fiber." *Medical Physics* 50.5 (2023): 3184-3190.

[27] Sarrut, D., Bardiès, M., Boussion, N., Freud, N., Jan, S., Létang, J. M., ... & Buvat, I. (2014). A review of the use and potential of the GATE Monte Carlo simulation code for radiation therapy and dosimetry applications. *Medical physics*, *41*(6Part1), 064301.

[28] Newhauser, W. D., & Zhang, R. (2015). The physics of proton therapy. *Physics in Medicine & Biology*, *60*(8), R155.

[29] National Nuclear Data Center, Nuclear Science References, version 4.1(2020). Information extracted from the NSR database (janisweb). [JANIS (oecd-nea.org)].

**Sree Bash Chandra Debnath** is currently a MSCA Global Post-doctoral research fellow at Aix-Marseille University- LP3, CNRS. He received his PhD from Aix-Marseille University under Marie Curie Fellowship in Medical Physics and Material Science Engineering in 2020. He is engaged with several collaborative research projects includes Physics research group of CINaM, Aix-Marseille University, IPC Cancer Hospital, France and Argonne National Laboratory, USA. He received his M.Sc and B.Sc in Engineering degree from University of Trento, Italy (2016) and Chittagong University of Engineering & Technology, Bangladesh (2011). His work focuses on medical dosimetry, optics, radiotherapy, X-ray, LINAC modelling and inorganic detector, Instrumentation and Signal Processing. Dr. Debnath is a member of IEEE, ESTRO and ASTRO.

**David Brasse** has been a Research director level 2, CNRS, IPHC UMR 7178 since 2012. He is the author of two book chapters, more than 70 peer reviewed articles, and 2 patents. His research interests include micro-dosimetry, proton therapy, PET imaging and SPECT system, radiation therapy, Interface between Physics, Biology, Medicine – Preclinical instrumentation. He obtained his PhD in Physics, Paris V University. PET imaging using SPECT system. Dr. David was awarded the Scientific Excellence award from CNRS in 2018.

**Didier Tonneau** is a Full Professor in Physics, Aix-Marseille University and Head of X-tip research group, CINaM. He graduated of Ecole Nationale Supérieure de Physique de Grenoble (ENSPG-1984) and achieved his PhD from University of Grenoble in Material - -Sciences in 1988. Currently, he is co-author of about 90 peer-reviewed articles and 5 patents. Prof. Tonneau was coordinator of several European projects, projects granted by French Ministry of Research, IDEX projects and a Laureate of Fulbright foundation in 2017. His

**Kevin Lalanne** is a research engineer at Institut de Radioprotection et de Sûreté Nucléaire, IRSN, PSE-SANTE/SDOS/LMDN, Cadarache, Saint-Paul-lès-Durance, France. He received his PhD from Aix-Marseille University in Nuclear Physics and Material Science in 2023 while working as a researcher with IRSN, CEA Cadarache, France. He research work focuses on Nuclear physics, Particle physics, Radiation protection, and Modeling

**Gael Simon** is currently a PhD student in the Hadrontherapy team at Radiobiology, Hadrontherapy & Molecular Imaging Department (DRHIM), Institut Pluridisciplinaire Hubert Curien - Strasbourg at Institut Pluridisciplinaire Hubert Curien – Strasbourg, France. His expertise encompasses of GATE simulations, GEANT4, Radiobiology, Proton therapy, and imaging.

current research focuses on fibered probes for medical physics (dosimetry in nuclear medicine), optics, Instrumentations, micro-electronics and X-ray spectrometry.

**Julien Darreon** works as senior Medical Physicist at Paoli-Calmettes Institute in Marseille, France, since 2011, INSTN-CEA graduate. He obtained his master's degree in physics from Paul Sabatier Toulouse University in 2006, and his Ph.D. degree in nuclear physics from Paris XI Orsay University in 2010, doing research at IRSN-CEA in Fontenay-aux-roses. His research interests include radiation dosimetry and planification (SBRT) in radiotherapy and nuclear medicine with a special interest for small field dosimetry and measurement using scintillator.
Dr. Darreon is treasurer and member of the administration council of the French Association of Physicists in Medicine (SFPM).

**Marc Rousseau** is an associate professor at Institut Pluridisciplinaire Hubert Curien (IPHC), CNRS, Strasbourg. He received his PhD degree in nuclear physics in 2000.

Dr. Marc is the author of more than 90 journal peer reviewed articles. His research interest is in Instrumental research & development for applied nuclear physics in the field of health.

**Francois Vianna-Legros** is a Researcher at Institut de Radioprotection et de Sûreté Nucléaire, IRSN, PSE-SANTE/SDOS/LMDN, Cadarache, Saint-Paul-lès-Durance, France. He is managing the Scientific and technical installation of MIRCOM facilities. He obtained his PhD degree in Nuclear Physics from Université de Bordeaux in 2014 and Masters in 2010 from the same university. His expertise encompasses nuclear physics, proton beam, high energy physics, dosimetry, hadron therapy, etc.

**Carole FAUQUET** received her PhD from Sorbonne Universités (Paris 6, France, 1992) and then joined Prof. W. R. Salaneck in the Surface Physics and Chemistry group (Linköping University, Sweden) as a post-doc fellow. Currently, she is an associate professor in Physics, Aix-Marseille University- CINaM, CNRS, France. Her current research interests include detectors design and characterization for environmental and medical applications.